Non-reciprocal phase transition enables swarming motility in biological active matter

Askin Kocabas

akocabas@ku.edu.tr

Koç University https://orcid.org/0000-0002-6930-1202

Sahin Ozdemir

Pennsylvania State University https://orcid.org/0000-0002-2625-3992

Mustafa Basaran

Koç University

Tevfik Yüce

Koç University

Ali Kecebas

Department of Engineering Science and Mechanics, and Materials Research Institute

Baha Altın

Koç University

Yusuf Yaman

Koç University

Esin Demir

Koc University

Coskun Kocabas

University of Manchester

Article

Keywords:

Posted Date: March 12th, 2024

DOI: https://doi.org/10.21203/rs.3.rs-3956047/v1

Additional Declarations: There is **NO** Competing Interest.

Non-reciprocal phase transition enables swarming motility in biological active matter

Authors

Mustafa Basaran[1,2,3], Tevfik Can Yüce[2], Ali Keçebaş[4], Baha Altın[1], Yusuf Ilker Yaman[1,3], Esin Demir[2] , Coşkun Kocabaş[5], Şahin K. Özdemir[5]†, and Aşkın Kocabaş[1,2,6,7]†

[1]Department of Physics, Koç University, Sarıyer, 34450 Istanbul, Turkey

[2]Bio-Medical Sciences and Engineering Program, Koç University, Sarıyer, 34450 Istanbul, Turkey

[3]Current adres: Sciences and Engineering Program, Harvard University, Cambridge 02138, MA

[4]Department of Engineering Science and Mechanics, The Pennsylvania State University, University Park, 16802, PA

[5]Department of Materials, University of Manchester, Manchester, M13 9PL, UK

[6]Koç University Surface Science and Technology Center, Koç University, Sarıyer, 34450 Istanbul, Turkey

[7]Koç University Research Center for Translational Medicine, Koç University, Sarıyer, 34450 Istanbul, Turkey

†Corresponding author: sko9@psu.edu , akocabas@ku.edu.tr

Abstract

Nonreciprocal interactions break action-reaction symmetry in systems of interacting bodies. This process inevitably introduces non-Hermitian dynamics which with its hallmark signature called exceptional points (EPs) has been a subject of intense research across different disciplines ranging from photonics to metamaterials. Whether non-Hermiticity and EPs are a fundamental property of nature and if so, how nature utilizes them to gain competitive advantage have remained largely unanswered. Although biological systems feature many examples of non-reciprocal interactions with the potential to drive non-Hermitian dynamics, these are often theoretically overlooked and not experimentally investigated. Here, we demonstrate in an active matter composed of social animal *Caenorhabditis elegans* and bacteria, non-Hermitian dynamics, and the emergence of EPs owing to the nonreciprocal nature of oxygen sensing, nonequilibrium interfacial current, and bacterial consumption. We observed that when driven through the EP, the system collectively breaks parity-time (PT) symmetry leading to traveling waves and arrested phase separation. We further find that these features enable the collective ability to localize interfaces between broken and exact PT-phases. Remarkably, this ability provides a strong evolutionary advantage to animals living in soil. Altogether our results provide mechanistic insights into the detailed symmetries controlling the collective response of biological systems; answer a long-standing problem; and give an example of the EP-enabled dynamics in a biological system.

Introduction

Active matter systems consist of numerous energy-generating or consuming components, thus they are intrinsically out-of-equilibrium[1,2]. In these intricately coupled systems, independent interaction channels such as drift-diffusion processes, sensing, and social norms, naturally give rise to non-reciprocity[3-10] where the constituents of the system affect each other differently. This apparent violation of Newton's third law[11], which states action-reaction symmetry, is a common feature in active matter. This is especially true for biological systems which generally have multiple active and passive components (e.g., cells, dense swarming animals, growing tissues, and environmental matrix). Recent studies have shown that nonreciprocity (i.e., action-reaction symmetry breaking) plays a key role in collective behaviors in active matter and leads to many exotic phenomena, ranging from synchronization and flocking to dynamic pattern formation. Combining the framework of nonreciprocity and the interacting active material platforms promises to provide a powerful toolbox to dissect the complexities of living biological materials.

While nonreciprocity arises naturally in active material and biological systems, in many fields of science and engineering (e.g., optics, electronics, acoustics, etc.) one has to deliberately break time-reversal symmetry to induce nonreciprocal electromagnetic wave transmission or nonreciprocal interaction between the subcomponents of a system. This is often achieved through strong nonlinearities, space- and/or time-dependent modulation of constitutive material properties, and magneto-optical components. Most recently, nonreciprocal interactions and coupling have emerged as a resource for building highly sensitive sensors[12-14]; achieving unidirectional perfect absorbers; and suppressing and enhancing spontaneous emission, to name a few. Nonreciprocal interactions bring about non-Hermitian dynamics, which suggests the toolbox developed for

studying non-Hermitian systems and the exotic features emerging from their EPs could be utilized in understanding and controlling complex active matter and biological systems.

Non-Hermiticity has its roots in quantum mechanics[15,16] and has been extensively studied in photonics[17], electronics, acoustics, optomechanics[18,19], superconducting qubits[20], trapped ions[21,22], single-spin systems[23], and in light-matter interactions[24]. Although in the majority of classical and quantum systems, non-Hermiticity and EPs emerge by judiciously controlling gain-loss balance as in active parity-time (PT) systems, dissipation- or loss-imbalance as in passive PT systems, and coupling strength among the couples, most recent studies have highlighted nonreciprocal coupling and interactions engineered using precisely located and controlled asymmetric scatterers or reflectors as a resource for non-Hermiticity[12,25,26]. In contrast to these artificially induced non-Hermiticity and PT symmetry, the majority of biological interactions are inherently nonreciprocal or asymmetric, and thus their dynamics can be modeled using effective Hamiltonian and dynamical matrix formalism widely used for non-Hermitian systems. Clearly, having nonreciprocal interactions, the active matter and biological systems should also have EPs and associated processes. Establishing this connection does not only allow studying complex biological systems using the well-known techniques utilized in non-Hermitian physics but it also will help answer the foundational question: How does the presence of EPs affect the dynamics of active matter and biological systems? Do presence of EPs and PT-symmetry breaking bring any advantage in biological systems? Despite significant progress in non-Hermitian physics and separately in active matter and biological systems, there is still a need for experimental platforms that bring together all these concepts to answer the above questions and reveal the potential biological implications of PT-symmetry, non-Hermiticity, and EP physics. Here we address this need and present experimental signatures of what happens to a biological system if it is driven

through an EP between exact- and broken-PT phases, and how this affects the system's collective behavior.

In this study, we investigated the detailed nonequilibrium process together with the concept of nonreciprocity controlling the collective behavior of animals using *C. elegans* as a model organism. These animals come together and feed on bacteria lawns. This intriguing collective response is known as social feeding behavior[27-29]. The physics of this collective routine is remarkable because the mixture of active worms and passive bacteria forms a highly interacting multi-component condensate. This active mixture forms social groups during feeding. Previous genetic studies have linked this feeding behavior to oxygen sensing[28,30], which promotes tracking low oxygen levels to locate bacteria as food. More interestingly, during their domestication process[31] as model organisms in the lab, the natural isolates of these social worms acquired several genetic mutations that significantly altered their oxygen preferences. As a result, social strains became solitary in the lab. Taken together, this collective behavior and the variability of their social response provide a valuable experimental system to study the detailed non-equilibrium dynamics of this interacting active matter system.

We found that all theoretically predicted non-Hermitian features, some of which are already observed in non-biological systems, including arrested coarsening, transitions between traveling and standing waves, and edge localization and delocalization emerge in these social animal groups. Using the approach learned from non-Hermitian physics in a non-equilibrium regime, our findings shed light on understanding the complex behaviors of biological systems including their evolutionary significance.

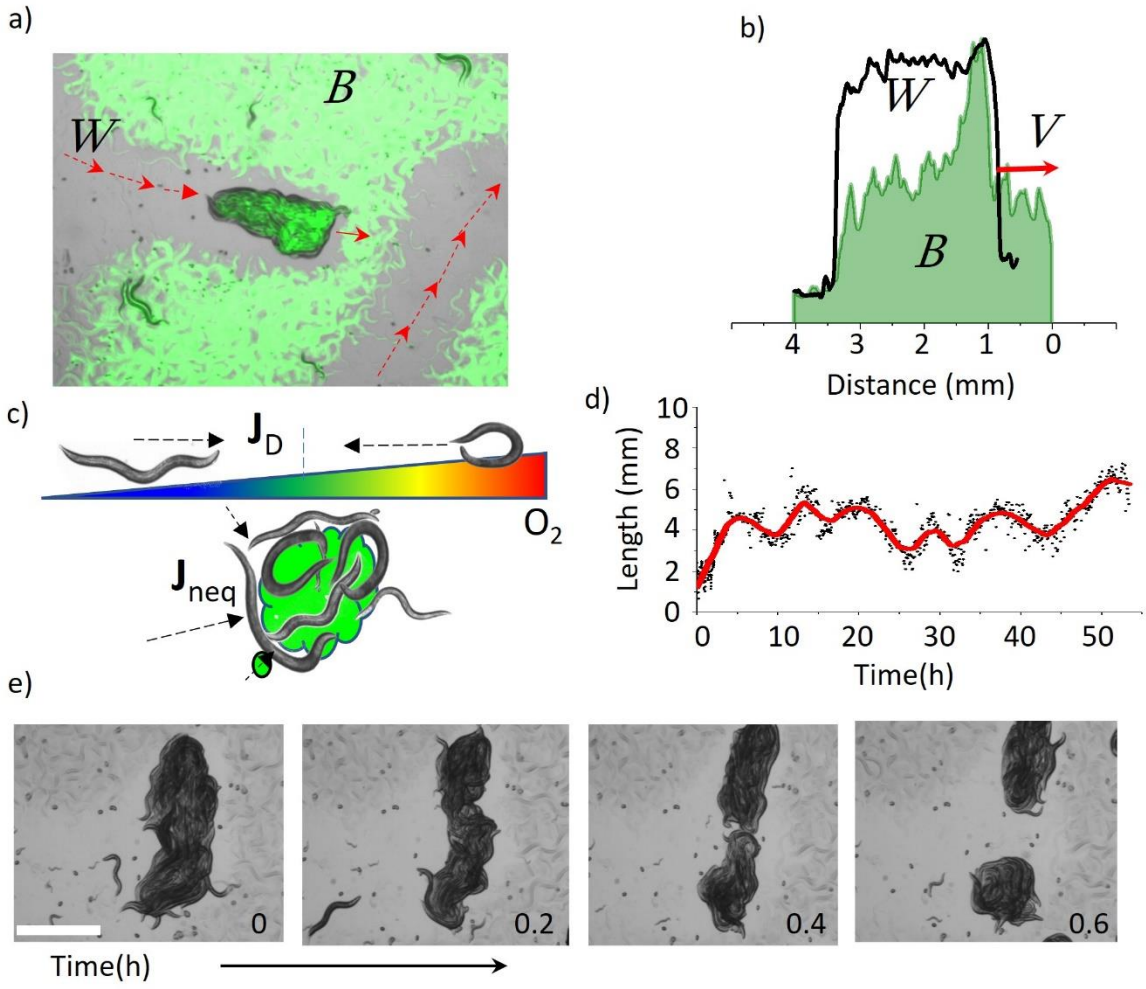

Figure 1 Emergence of a traveling wave state in an active worms-bacteria mixture. a) *The image of a worm aggregate overlaid with a GFP-labeled bacterial field, where a group of worms is swarming together.* ***b)*** *Densities of the worm W and bacteria B fields, revealing the asymmetric profile during the traveling state. V represents the forward velocity of the animal group.* ***c)*** *Schematic representation of how active worm aggregates concentrate bacteria by coming together on a bacteria lawn and reducing oxygen levels. Conversely, aggregated worms can drift bacteria across the interface. This process could be represented by two material currents J_D and J_{neq} .* ***d)*** *The size of the worm aggregate as a function of time indicates the arrested coarsening during the traveling state.* ***e)*** *Splitting of worm aggregate into smaller parts limiting the growth of the aggregate size. Scale bar, 1mm.*

Results

Experimental observation of the traveling state of coupled worms and bacteria mixture

To study the physics of social feeding behavior involving bacteria, we used time-lapse microscopy to observe worms (***W***) and bacteria (***B***) densities together (Fig. 1). We used the Green Fluorescent protein (GFP) to label the bacteria so that we could observe the worms and bacteria separately. Over the course of several days of imaging starting from a single worm, we observed the formation of small groups of animals traveling on the bacteria lawn (Figure 1a, Supplementary Video1-2). During this traveling state, the worms and bacterial fields showed various configurations, including colocalization, delocalization, and asymmetric density distributions (Figure 1b). Of particular interest is the asymmetric density profile, which arises when the animals are placed on a flat and uniform bacterial lawn. In this scenario, the swarming animals can spontaneously develop a bacterial gradient and move towards regions with higher bacterial density.

In a previous study[32], we observed that when worms aggregate, they can cause bacteria to concentrate within the aggregates, leading to the formation of complex dynamical patterns. Initially, we attributed this to the low oxygen taxis behavior of the worms, which caused the bacteria to co-locate due to the sponge-like structures in the animal groups (Figure 1c). However, it turned out that the process was more exotic, and was purely driven by their activity. This colocalization process was the first dynamical feature that prompted us to investigate the active matter nature of the worm-bacteria mixture, which was likely responsible for the observed phenomena. In this study, we further focused on several other experimental observations that suggested that this process was particularly triggered by a nonequilibrium and hence non-Hermitian process in the animal groups.

Another signature of non-equilibrium behavior we noticed in this animal model is the arrested size of the active worm aggregates (Figure 1d). Animal groups can merge together, but if they form larger groups, they later split into smaller parts (Figure 1e, Supplementary Video 3). The arrested coarsening dynamics of the active system is of special importance because the process limiting the universal coarsening event requires critical dynamics. The most parsimonious hypothesis explaining this observation is that the interface of the worm aggregates generates a nonequilibrium bacterial current ($\mathbf{J_{neq}}$) that could limit the coarsening process[33].

Finally, we observed that the worm-bacteria condensates were highly vulnerable to local depletion of bacterial densities, leading to the formation of bubbles (Supplementary Video 4). These observations share some similarities with the recently developed active model B+[34], also known as bubbly phase separation, which is based on a single active component. However, it is important to note that our system differs from one-component active platforms due to the coupling of the worm and bacterial fields. Despite this difference, the macroscopic dynamics of hole formation in the worm-bacteria mixture were found to be similar. These three experimental findings support the idea that the worm-bacteria active system exhibits special nonequilibrium dynamics that control their collective behaviors, but they do not tell whether EPs exist in this model system and what roles EP, if exist, and PT-symmetry breaking play in the observed behaviors.

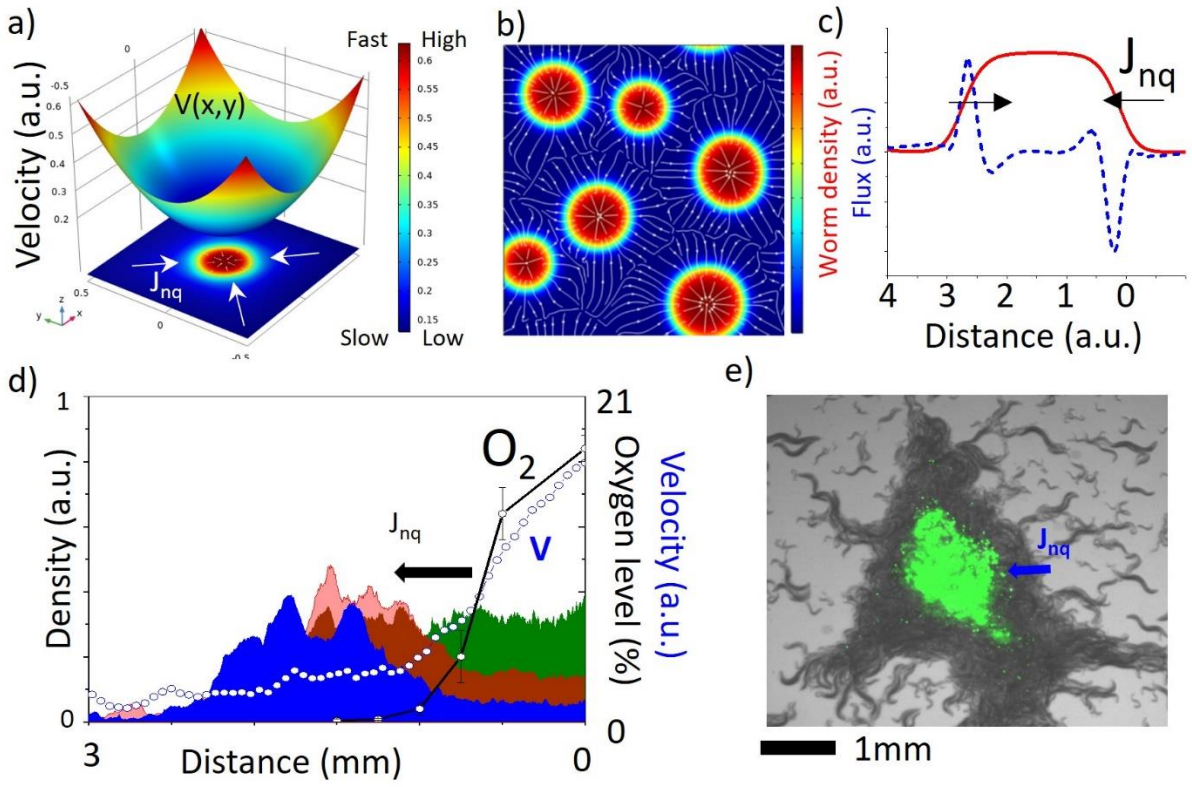

Figure 2: Spatial activity gradient generates non-equilibrium interfacial current on the passive component. ***a)*** *Numerical simulation demonstrating the drift process driven by a velocity gradient in space.* ***b)*** *Simulation result showing the aggregating active worms generate a velocity gradient across the interface, resulting in a drift current* J_{nq}. ***c)*** *The cross-sectional profile of worm density and the corresponding nonequilibrium drift current.* ***d)*** *Experimental results demonstrating the interfacial drift current of passive beads from the oxygen-lacking edge to the oxygen-depleted center of the group. Aggregating worms and self-consumption decrease oxygen concentration and generate a spatial activity gradient. Green (initial) to blue (final) colors indicate the time and bead distribution towards low oxygen regions where the animals are slow.* ***e)*** *A typical image of a worm aggregate overlaid with concentrated passive green fluorescent beads at the center of the group. Note that worm and bead densities are colocalized. Oxygen and velocity profiles are given in Supplementary Figure1.*

Spatial activity gradient generates non-equilibrium interfacial current

To further assess the nonequilibrium process at the interface of the worm-bacteria mixture, we performed numerical simulations. We found that the speed of the worms was strongly dependent on the oxygen concentration, while the bacteria were passive constituents of the system that exhibited only small fluctuations. Due to hydrodynamic coupling with the bacteria, the worms were capable of inducing strong activity at large scales, leading to bacterial drift and spatial variations in the speed at the interface[35-37] (Supplementary Video5).

It is important to note that this process involves the coupling of large active worms (~1mm) and small passive bacteria (~5μm), which is critical due to the different types of drift mechanisms that originate from the size difference between the interacting components. First, under a spatial activity gradient, small active matter can apply active phoretic pressure to larger passive components, as seen in the centering of the nucleus in a cell, where the activity gradient around the cortex pushes large particles towards the center[38,39]. Additionally, at the cellular membrane, the dynamic coupling between large cargo proteins and the active MinB system can also be described as an example of phoretic active pressure[40]. From this perspective, our system exhibits different dynamic processes. The second type of drift originates from the spatial activity dictated by large active particles. It is worth noting that the response of particles to activity gradients has received significant scientific attention and has been theoretically well-studied[35,41]. Our system should be considered in this class.

To better understand the dynamics of the interaction between large active worms and small passive bacteria at interfaces, we simulated bacterial diffusion, where the speed of the passive bacteria is dictated by the active worms. The worms can also self-aggregate due to local oxygen depletion, which we modeled by using the same principle of motility-induced phase separation, resulting in

negative effective diffusion[42,43] ($D_{eff} < 0$, Supplementary Note section 1, Supplementary Video 6). This self-aggregation condition can be seen as the first of two instabilities required for non-reciprocal phase transitions. As expected, the activity gradient at the interface generates a drift current, causing the passive particles to be pumped toward the center of the aggregates (Figure 2a-c, Supplementary Video 6). We observed the same process even when bacteria were replaced with polymer beads, further confirming the nonequilibrium nature of the process (Figure 2d-e, Supplementary Figure 1). The dense worm aggregates depleted oxygen, leading to the formation of oxygen and velocity gradients at the interface, which pumps the passive beads toward the center. We observed similar nonequilibrium interface currents and co-localization of active and passive components at a larger scale (Figure 2e). Based on these experimental findings and numerical results, the dynamics of the entire process can be reduced to a flux term at the interface, which we modeled using $J_{neq} = \zeta B \nabla W$ (Supplementary Note section 2).

Emergence of exceptional points and traveling state in worm-bacteria mixture

To gain more intuition about the coupled dynamical system between worms and bacteria and study how EPs emerge in this dynamics, we formulated a set of coupled drift-diffusion equations for two conserved density fields, $\boldsymbol{W}$ and $\boldsymbol{B}$. The time evolution of the worm density is influenced by both oxygen-dependent motility and the interaction between worms and bacteria. These dynamics can be expressed mathematically as follows:

$$\frac{\partial W}{\partial t} = \nabla \cdot \left[D_{eff} \nabla W + \beta W \nabla B \right] - \gamma_W \nabla^4 W$$

$$\frac{\partial B}{\partial t} = \nabla \cdot \left[D_B \nabla B - J_{neq} \right] - \lambda W B - \gamma_B \nabla^4 B$$

where $\boldsymbol{D_{eff}}$ represents the motility-dependent dispersion of worms which is negative and promotes self-aggregation, $\boldsymbol{D_B}$ is the diffusion coefficient of bacteria induced by active worms, and $\beta = \frac{v}{\tau}\frac{\partial v}{\partial B}$ is the aerotactic coupling coefficient indicating the strength of the animal response to the bacteria-dependent oxygen gradient. Note that λ is the bacterial consumption by the worm and γ is the phenomenological surface tension parameter. v and τ are the velocity and reversal rates of the animals.

As a new cross-coupling term we added non-equilibrium flux ($\overrightarrow{J_{neq}} = \zeta B \nabla W$) which is the first term breaking the reciprocity between worms and bacteria. When we linearize the system around equilibrium points, the dynamical matrix can be simplified to the version given below, which shares the common form of the coupled dynamical system widely used in non-Hermitian physics (Supplementary Note section 3)

$$\frac{\partial}{\partial t}\begin{bmatrix}\rho_W \\ \rho_B\end{bmatrix} = \begin{bmatrix}D_{WW} & D_{BW} \\ D_{WB} & D_{BB}\end{bmatrix}\begin{bmatrix}\rho_W \\ \rho_B\end{bmatrix}$$

D_{BW} is the cross-diffusion term and represents the chemotactic drift of the worms across the bacterial gradient. This term is controlled by the oxygen concentration which is defined by the local bacterial density. Further, the other cross-diffusion term D_{WB}, absorbs non-equilibrium interface flux ($\overrightarrow{J_{neq}}$) promoting colocalization and also the consumption rate of bacteria (λ) by the worms which acts as a delocalization term in the system. The schematic representation of these interactions between worms and bacteria is given in Figure 3a. Eigenvalues $\sigma_{\pm} = (D_{WW} + D_{BB})/2 \pm \sqrt{\xi}/2$ where $\xi = (D_{WW} - D_{BB})^2 + 4D_{WB}D_{BW}$ reveals the pseudo-Hermitian[44] characteristic of the system (Supplementary Note section 3,4) with the emergence of

an EP at $\xi = 0$ where both the eigenvalues and the associated eigenvectors coalesce. EP divides the parameter space into three: i) $\xi = 0$ where eigenvalues are degenerate (i.e., critically damped harmonic oscillator); ii)) $\xi < 0$ eigenvalues become complex conjugate pairs (i.e., underdamped harmonic oscillator) and the system oscillates; and iii)) $\xi > 0$ where two distinct eigenvalues emerge and the system approaches the equilibrium position without any oscillation (i.e., overdamped harmonic oscillator). We note that the emergence of EP is the second instability indicating the Parity-Time (PT) symmetry-breaking conditions (Figure 3b, Supplementary Note section 4,5). The eigenvalues of the system be simply controlled by two critical external parameters; consumption rate λ of bacteria by worms which can balance the bacterial pumping into the worm aggregates and also ambient oxygen level that controls the activity and the sensitivity of the worms. The corresponding phase space has three major domains, uniform densities, static pattern forming, and traveling state regions (Figure 3b top). To further test the theoretical predictions, we numerically solved the coupled system in two dimensions (2D) (Supplementary Video 7). We observed that static colocalized (aligned), delocalized (antialigned) patterns, and traveling (chiral) states emerged during the simulation (Figure 3c). We then repeated the simulations by implementing local initial noise to trigger the first aggregation instability and observed the dynamics of localized individual groups traveling toward bacteria-available regions (Figure 3d). The system spontaneously breaks spatial symmetry and develops a self-generated bacterial gradient profile (Figure 3e). This broken symmetry further guides animal groups into spontaneously picked outward directions (Supplementary Video 8,9). When we plot the density profiles of worms (W) and bacteria (B) the broken symmetry and stable phase difference between these fields become more evident (Supplementary Note section 4). This phase difference also

indicates the chiral state formed by the worm bacterial fields. Simply, worms are chasing the self-generated bacterial gradient profile.

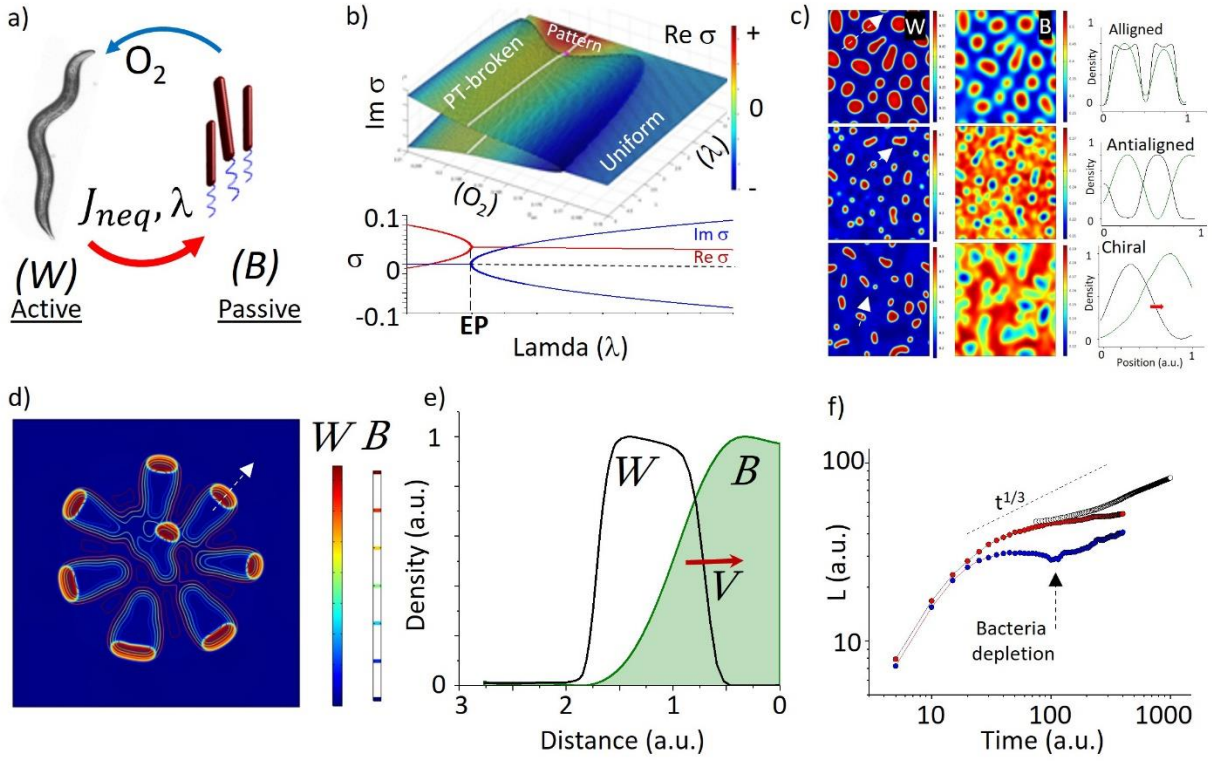

Figure 3: Emergence of exceptional points (EPs) in nonreciprocally interacting worm and bacterial active mixture. a) *Schematic representation of a two-component active matter system consisting of worms (W) and bacteria (B). Non-equilibrium fluxes control the time evolution of the system by promoting colocalization and bacterial consumption λ drives the delocalization process of worm and bacterial fields. Due to aerotaxis, the depletion of oxygen by the bacteria controls the worm's activity.* ***b)*** *Numerical simulation of the phase diagram of the coupled active matter mixture indicating three different domains. The system dynamics depends on the critical coupling parameter λ and the ambient oxygen level. Above a critical level, the eigenvalues of the system develop complex conjugate pairs (bottom). The emergence of the complex conjugate pairs drives the traveling state of the patterns (PT broken region).* ***c)*** *Worm and bacterial fields show aligned (colocalized) and antialigned (delocalized) profiles before forming the traveling state (chiral). Intensities are measured across the arrows.* ***d)*** *Numerical simulation of the worm aggregates traveling across uniform bacterial density (contour).* ***e)*** *Simulation results of worm and bacterial densities indicating the asymmetric density profile above EP indicating the PT-symmetry breaking between worm bacteria fields.* ***f)*** *The coarsening process of the worm aggregation is arrested (Blue). Numerical simulation indicates the separate impact of bacterial consumption (red) and interface current on the coarsening dynamics. Black dots represent the result of the universal coarsening process without bacterial current and consumption.*

As a final stage of the numerical simulations, we analyzed the coarsening dynamics of the worm bacteria mixture under various conditions. We first tested the characteristic size of the groups above the EP where the aggregates are moving. As expected in this regime the coarsening is arrested (Figure 3f). This arrested state is easily understood by considering the bacterial flux around the periphery of the groups. As groups grow in size the interface has to pump more bacteria to maintain the low oxygen level around the favorable range. Above the critical size; however, bacteria get depleted due to high consumption and oxygen level increases which further promotes high motility. The increase in the motility increases the diffusion and finally breaks the groups into small parts as we observed in our experiments. In the case of worm condensate (Supplementary Video 4), high consumption of bacteria could locally trigger the oxygen increase and the final system could drive the formation of holes. This point is the similarity between our system and the active Model B+. The susceptibility of the system against local noise is mainly triggered by the imbalance between inward bacterial pumping and oxygen increase. We also tested the coarsening scenario without bacterial consumption ($\boldsymbol{\lambda = 0}$) while keeping nonequilibrium pumping on ($\overrightarrow{J_{neq}}$). Interestingly the system shows different scaling. We hypothesize that this suppression is controlled by the interface current of bacteria in the aggregates. Finally, we noticed that removing all the cross-coupling terms between worms and bacteria gave rise to the formation of regular motility-induced phase separation with a universal coarsening profile ~$t^{1/3}$ (Figure 3f). All these numerical results support that the active worm and bacteria mixture has non-Hermitian features and shows all expected dynamical properties including EPs, traveling state, and arrested coarsening process. Nonequilibrium interface current and bacterial consumption together spontaneously breaks PT symmetry leading to the emergence of a collective traveling state of the worm aggregates across

uniform bacterial density. The similarities between theoretical expectations and the experimental results are remarkable.

Edge localization and evolutionary significance

One of the interesting observations in topological physics is the formation of localized edge states at the interface of two topologically different domains[45-49]. Such edge states could also emerge in non-Hermitian systems. Recent theoretical studies have elaborated on the possibility of such dynamics in various biological networks[47-49]. In this study, we aim to bring a different perspective to this concept. We realized that interfaces are very common environmental features in nature, such as water-soil interfaces in lake sediments or air-soil interfaces on the ground surface of forests. These interfaces are the main battlegrounds between competing animal species. Different regions of these interfaces may have separate challenges or predators, and staying locally around them could provide specific advantages. Similarly, soil nematodes, *C. elegans,* live in wet soil where the fluids are decomposing. Understanding the collective response of the worms at these interfaces (Figure 4a) may link the physics of localized edge states and their potential biological implications.

In order to elucidate topology in interacting biological systems, we studied the dynamics of worms, specifically their behavior around interfaces representing different symmetries in the phase space. We selected the interface between exact and broken PT domains which were obtained by partially blocking oxygen penetration from the air. The numerical results showed the localization of animals along the interface (Figure 4b and Supplementary Video10). In our experiment, we placed a cover glass on a bacteria lawn with swarming animals and observed their collective responses. Our findings indicate that interfaces can lead to the emergence of localization at the sharp interface where oxygen concentration quickly shifts from high (normoxic) to low (anoxic) levels. Neither

side of the interface is favorable for single worms; the open region has high oxygen levels (i.e., broken PT phase) and is open to predators, while the closed region has very low oxygen levels (i.e., exact PT phase) due to the presence of bacteria and blocked oxygen penetration. However, at the interface, animals can spot favorable conditions and localize by slowing down (Figure 4c, Supplementary Video11). This raises the question of whether localization provides an evolutionary advantage. To test this hypothesis, we designed a new experiment to mimic the granular structure of the soil, the natural habitat of *C. elegans*. We used gel-based beads (Sephadex 50) soaked in bacterial suspension (as shown in Figure 4d), which has low oxygen levels but provides more interfaces for worms to stay around. To test the worms' preference, we extended the bacterial lawn to an open region without interfaces. We found that the majority of social worms (npr-1) quickly found and preferred staying in the granular region when placed away from it, while solitary strains (N2) showed a different response, spreading around without a clear preference for this region (Figure 4e, Supplementary Video12). Based on these observations we can conclude that the natural isolate of *C. elegans,* aka social strain*,* prefers staying at the interfaces where they can get sufficient oxygen while keeping themselves from open regions. When they get into the open region they come together and collectively form groups by decreasing internal oxygen levels. Interestingly solitary strain N2 which evolved in the lab on a flat surface lost this collective response and interface tracking ability.

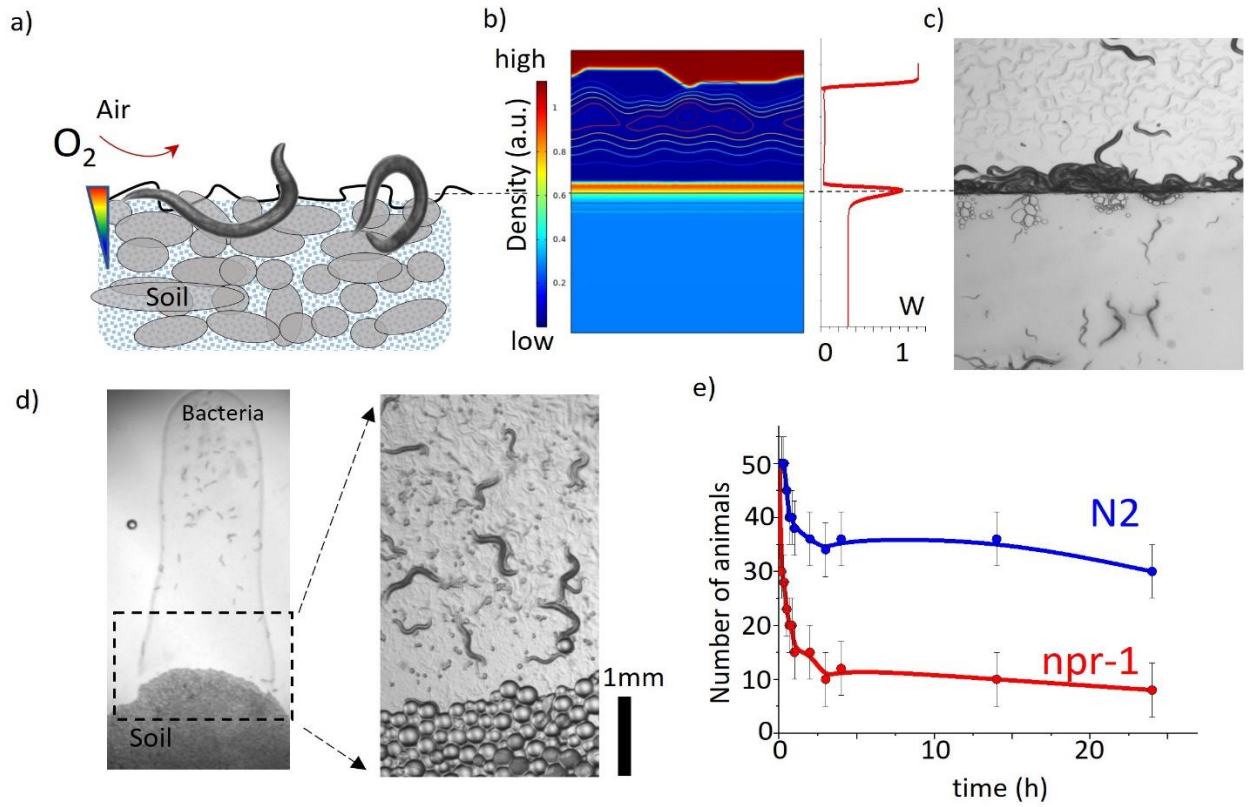

Figure 4: Evolutionary significance of edge localization of social animals at the interface between different domains. a) *Schematic representation of an air-soil interface corresponding to uniform and traveling states of the phase diagram.* ***b)*** *Numerical results of the coupled worm-bacteria system localizing around the edge of the air-soil interface are shown.* ***c)*** *Experimental result of the localized edge state at the interface generated by blocking oxygen penetration.* ***d)*** *Image of the experimental platform used to test the ability to localize around the edge. Polymer beads are used to generate a multilayered structure to mimic the soil-air interface.* ***e)*** *Social animals prefer staying in the granular region where they can hide and stay around the edges. However, solitary animals spread around and do not show any edge preference.*

Discussion

Nonreciprocity, a characteristic phenomenon observed in interacting biological entities—from bacteria to birds in flight—is inevitable in nature. Influenced by various factors like social interactions, restricted perceptual abilities, or hydrodynamics, this nonreciprocity plays a crucial role and serves as a bridge, linking the dynamics of biological systems to non-Hermitian physics, a field with significant applications in areas such as optics, electronics, acoustics, and quantum

mechanics. Such a combination provides a powerful toolbox for probing the complex dynamics of active matter, offering fresh insights into the intricacy of biological systems.

Non-Hermitian, including PT-symmetric, toolbox, and features offer a beneficial macroscopic metric to understand a system's response. In our study, we noted that PT symmetry breaking manifests as an arrested travel state of animal groups. This observation is critical since pattern-forming systems typically generate standing wave patterns with a universal coarsening response[50]. Traveling wave patterns akin to these have been studied in various physical systems, like viscous fingering[51], which necessitates two successive instabilities to produce traveling waves. The primary difference in active biological systems is their self-aggregating behavior, corresponding to the first instability. The role of nonreciprocity becomes particularly significant for the second instability, which spontaneously breaks PT symmetry and provides collective motility.

Moreover, we discovered that interface localization is a crucial difference between social and solitary animals. This response is indeed vital in nature but not in the lab due to the absence of the predators, and this finding illuminates why the solitary strain lost this ability during the lab domestication process. The most captivating aspect of physical systems is edge localization at the interface of two topologically different systems (i.e., the interface of systems with trivial and nontrivial topologies). This characteristic, emerging from topological constraints, allows for unidirectional propagation along the interface, showing resilience against external disturbances. Our findings also introduce new questions, like the chirality of localized animals at the interfaces having varying symmetries. We hypothesize that fluctuations of the localized state around the interface should propagate unidirectionally. Future investigations are necessary to explore these intriguing collective behaviors of animals.

In conclusion, different forms of nonreciprocity can be simultaneously observed in large microbial populations. Our findings hold potential relevance for comprehending the complex dynamics of these populations, from gut microbiota to ecological systems. We further speculate that the principles derived from non-Hermitian physics could illuminate the understanding of interactive biological systems.

Data availability

The critical experimental data generated or analyzed during this study are provided as supporting video files. We did not generate additional data sets.

Software availability

All the codes used in the study will be available online.

Materials and Methods

Microscopy imaging. Fluorescence time-lapse imaging was performed using Stereo SMZ18 microscopes. Images were obtained using Andor EMCCD camera. Time intervals between successive images were set to 5-15 minutes.

Oxygen Measurement

Oxygen level was measured by using a florescence-based fiber optic oxygen sensor (PreSens, Microx TX3). During [O2] measurements the sensor probe was precisely inserted between the cover and NGM surface by using a motorized stage. The fiber optic sensor has a polymer coating and the presence of O_2 quenches the fluorescence signal.

Numerical Simulation

COMSOL Multiphysics and finite element methods were used to solve the coupled partial differential equations. The coupled partial differential equations are implemented by using the general form of coupled differential equations.

C. elegans strains

Strains were grown and maintained under standard conditions. Nematode growth media (NGM) plates having a diameter of 9 cm were used for maintaining the worms. NGM plates were seeded with 1 ml of GFP labeled OP50 culture. To eliminate the thick edge formation of the bacteria lawn, 100 μg/μl ampicillin was added to the ngm plates. All the strains were obtained from Caenorhabditis Genetics Center (CGC). Two primary strains *npr1* (DA609), and N2 were used in the study.

Author contributions

M.B, Y.I.Y, and A.Ko. initiated the project. M.B. and A.Ko performed the experiments and developed the initial model. S.K.Ö, and C.K led the implementation of non-Hermitian and PT-Symmetry concepts. T.C.Y developed the theory and performed simulations, B.A and A.Ke verified the results. ED and A.Ko performed oxygen measurements. A.Ko. prepared the draft and all the authors contributed to the final writing of the manuscript.

Acknowledgments

This work was supported by Airforce Office of Scientific Research (AFOSR) under Grant No: FA9550-22-1-0431 with Program Manager Ali Sayir. S.K.O acknowledges the support from Air AFOSR Multidisciplinary University Research Initiative (MURI) Award No. FA9550-21-1-0202 We thank Livio N. Carenza, M. Işkın, and Alkan Kabakçıoğlu for critical reading of the manuscript.

Competing interests

The authors declare no competing interests.

Video Captions

Video 1 Time-lapse imaging of growing worms (strain npr-1, light1) on an OP50-seeded NGM plate. The video shows both bright-field images of the worms (left) and fluorescence images of the bacteria (OP50:GFP, right). As the animals form aggregates, they concentrate bacteria in the groups. Due to bacterial consumption, both concentrated and depleted bacterial profiles occur. At later stages, the groups begin to swarm after developing an asymmetric bacterial profile. The video is associated with Figure 1a.

Video 2 Magnified time-lapse imaging of swarming animal groups on a bacterial lawn. The fluorescence images of bacterial density show an asymmetric profile. As animal groups grow in size, they split into smaller parts. The video is associated with Figure 1b.

Video 3 Time-lapse imaging of a splitting event within an animal group. As animal groups grow in size, they split into smaller parts. The fluorescence image shows the asymmetric profile of the bacterial distribution within the group. The video is associated with Figure 1e.

Video 4 Time-lapse imaging of dense worm-bacteria condensate, where the worms are forced to form a dense swarming body around the edge of the bacterial lawn. Instead of forming a complete phase separation, the dense

swarm spontaneously forms holes triggered by local depletion of bacteria, leading to an increase in oxygen levels. This feature highlights the susceptibility of swarming animal groups to bacterial fluctuations.

Video 5 Simulation results of concentration and polarization of passive particles under a spatial velocity profile. The velocity profile is Gaussian, and particles slow down at the center. The video is associated with Figure 2a.

Video 6 Simulation results of self-aggregating animals and the emerging interface current of passive particles (streamline) around the edge of the groups. The video is associated with Figure 2b.

Video 7 Simulation result of a 2D coupled worm (color) and bacteria (contour) active mixture. Self-aggregation is triggered by initial spatial noise, and as animals aggregate, they gradually form traveling groups. This video demonstrates that the coupled worm-bacteria mixture forms a traveling state. The video is associated with Figure 3c.

Video 8 Simulation result of traveling multiple groups. Self-aggregation is triggered by local spatial initial noise. Traveling groups move outward.

Video 9 Simulation results of a single traveling group of animals. The animal group develops a bacterial gradient and travels towards the region with higher bacterial concentration. This video demonstrates the arrested group size and asymmetric bacterial profile. The video is associated with Figure 3e.

Video 10 Simulation result of an edge state localized at the interface between traveling and uniform domains of the phase diagram. The domains are established by modulating the ambient oxygen level, changing it from 21% to 0%.

Video 11 Experimental observation of the localization of animals around the edge of the glass cover, which blocks oxygen penetration on a bacterial lawn. The video is associated with Figure 4.

Video 12 Time-lapse imaging of solitary (N2, left) vs. social (npr-1, right) animals moving on a bacterial lawn with gel beads. Social animals quickly disperse and prefer staying in the granular region. Solitary animals disperse but do not show a clear preference.

Supplementary Figures

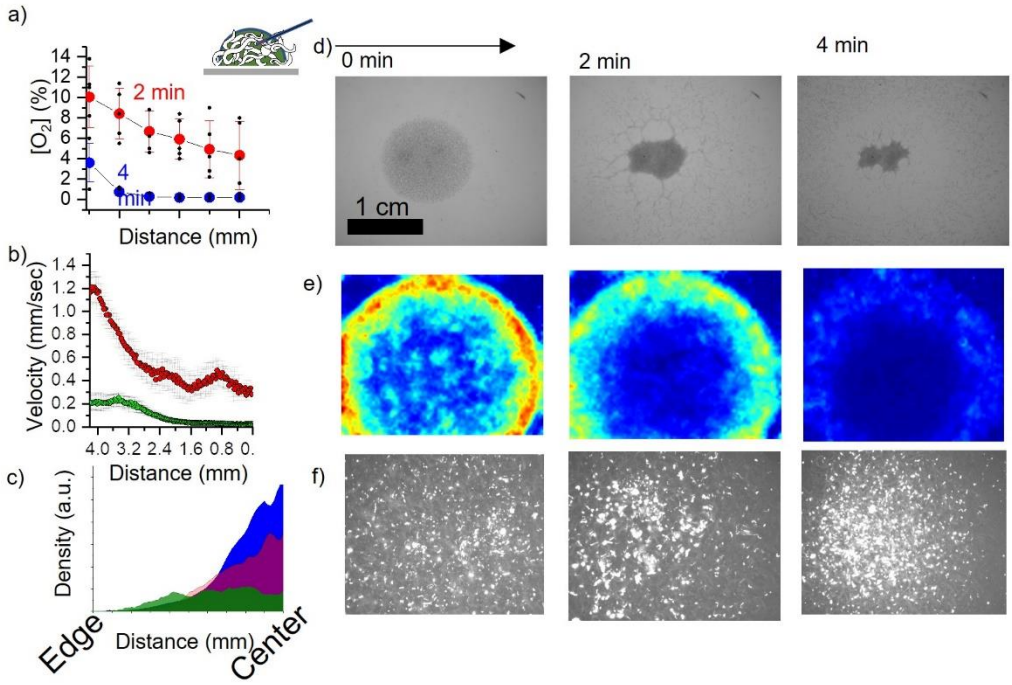

Supplementary Figure 1 Oxygen measurement vs speed distribution and colocalization of worms and passive beads. ***a)*** *Radial oxygen profile measured by fiber optic sensor across the worm droplet. A dense worm population generates oxygen gradient across the droplet by consumption.* ***b)*** *The velocity of the worms shows strong swimming activity around the edge of the droplet where oxygen is available.* ***c)*** *Active worms generate a velocity gradient across the interface, resulting in a drift current. Initially, uniform beads (green profile) accumulate around the center of the droplet.* ***d) e) and f)*** *are the images of the worms' activity and fluorescence beads in the droplet*

Suplementary Notes

I.General Equations of Worm and Bacteria Densities

We previously observed that the velocity of the social *C. elegans* strain depends on the oxygen level of the environment[32]. Animals slow down at favorable oxygen levels and the typical velocity profile is given below.

$$v(O) = \alpha(O - O_{in})^2 + v_0$$

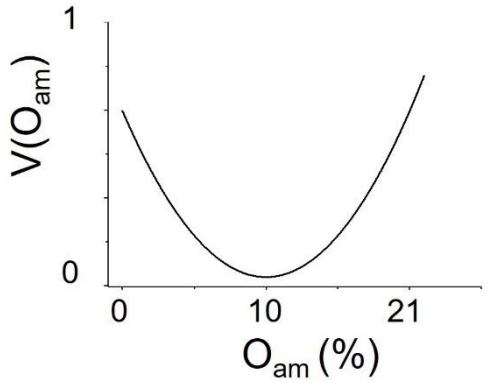

Supplementary Figure 2; Velocity profile of active worms as a function of ambient oxygen level. Worms slow down at an intermediate oxygen level.

The time evolution of the oxygen density is determined by the diffusion, penetration, and consumption of the oxygen by both the bacteria and the worms. These dynamics can be modelled as

$$\frac{\partial O}{\partial t} = D_O \nabla^2 O - k_B B - k_w W + f(O_{am} - O)$$

We assume that oxygen has a fast dynamical response compared to other timescales of active worm W and passive bacteria B. We can simplify the oxygen kinematics in a static manner as

$$O(W, B) = O_{am} - \frac{k_B}{f} B - \frac{k_W}{f} W + O(\nabla^2 O)$$

Further, we can use a static version of the oxygen level to define the velocity profile of the worm depending on both the worm and bacteria densities:

$$v(W,B) = \alpha(O_{am} - O_{in} - \frac{k_B}{f}B - \frac{k_W}{f}W)^2 + v_0$$

Finally, the drift-diffusion equation for the worm density using the Schnitzer's equation[37] as

$$\frac{\partial W}{\partial t} = \nabla \cdot \left[\nabla(\frac{v^2}{2\tau}W)\right] - \gamma_W \nabla^4 W$$

$$\frac{\partial W}{\partial t} = \nabla \cdot \left[\frac{v^2}{2\tau}\nabla W + \frac{v}{\tau}W\nabla v\right] - \gamma_W \nabla^4 W$$

Implementing the defined velocity profile of the worms and its dependence on bacterial densities, we can modify the time evolution equation as follows

$$\frac{\partial W}{\partial t} = \nabla \cdot \left[\frac{v^2}{2\tau}\nabla W + \frac{v}{\tau}\frac{\partial v}{\partial W}W\nabla W + \frac{v}{\tau}\frac{\partial v}{\partial B}W\nabla B\right] - \gamma_W \nabla^4 W$$

Finally, the equation can be further simplified by defining effective diffusion for W which can represent the self-aggregation process (negative effective diffusion). Further, the gradient of bacteria density drifts the worms and the sensitivity β is defined as

$$D_{eff} = \frac{v^2}{2\tau} + \frac{v}{\tau}\frac{\partial v}{\partial W}W$$

$$\beta = \frac{v}{\tau}\frac{\partial v}{\partial B}$$

Substituting the above expression into the time-evolution equation, we end up with

$$\frac{\partial W}{\partial t} = \nabla \cdot \left[D_{eff}\nabla W + \beta W \nabla B\right] - \gamma_W \nabla^4 W$$

II.Polarization of Bacteria field and Quasi Stationary Approximation

The second component of our dynamical system is the drift-diffusion process of the passive bacterial density, denoted by B. In addition to the classic diffusion process, the non-equilibrium

bacterial interface flux J_{neq} plays a significant role in the dynamics of B. To represent this interface current, we used the modified Toner-Tu equations[35], where $\bar{v}$ is the average velocity of the bacteria. The time-evolution of B can be written as

$$\frac{\partial B}{\partial t} = \nabla \cdot \left[D_B \nabla B - J_{neq}\right] - \lambda W B - \gamma_B \nabla^4 B$$

$$J_{neq} = \bar{v}\,\vec{P}$$

The first term on the right-hand side of the equation represents the diffusion of the bacteria. This process is influenced by the motion of animals, and localized bacterial densities can simply disperse due to the random movement of animals.

The second term represents the critical non-equilibrium flux resulting from the polarization of the bacteria due to hydrodynamic interactions with worms. Polarization represents the directional bacterial flux towards the center of the animal groups, caused by the spatial activity gradient. The third term is the non-conserved reaction term resulting from the consumption of bacteria by worms. The last term is the surface tension. The general equation for the polarization of bacteria is given as:

$$\frac{\partial \vec{P}}{\partial t} = -\frac{1}{2}\,\nabla(\overline{v}B) - \gamma_1 \vec{P} - \gamma_2 P^2 \vec{P} + k\nabla^2 \vec{P} - w_1(\vec{P} \cdot \nabla)\vec{P}$$

For the equation of the polar order of passive bacteria, we can use the quasi-stationary assumption, this is because the polarization of the bacteria occurs faster than the time scales of the worms. Since there is no significant self-advection and no intrinsic alignment preference, we can express the polarization in terms of the bacteria density and the average velocity $\overline{v}$, which is referred to as the active pressure term due to density and velocity gradient.

$$\vec{P} = -\frac{1}{2\gamma_1}\nabla(\bar{v}B)$$

Bacteria in this system are considered as passive particles, therefore worm activity drives bacterial velocity, we can use the following assumption;

$$\bar{v} = vW$$

where v is the velocity of the worms. If we use this velocity form in the polarization field of the bacteria, we then have the following expression for the bacteria order.

$$\vec{P} = -\frac{1}{2\gamma_1}\nabla(vWB)$$

$$\vec{P} = -\frac{1}{2\gamma_1}\left[\mathrm{WB}\nabla v + vW\nabla B + vB\nabla W\right]$$

$$\vec{P} = -\frac{1}{2\gamma_1}\left[WB\left(\frac{\partial v}{\partial B}\nabla B + \frac{\partial v}{\partial W}\nabla W\right) + vW\nabla B + vB\nabla W\right]$$

$$\vec{P} = -\frac{1}{2\gamma_1}\left[\left(WB\frac{\partial v}{\partial B} + vW\right)\nabla B + \left(WB\frac{\partial v}{\partial W} + vB\right)\nabla W\right]$$

Finally substituting the above equations in the expression for time evolution of the bacteria density, we obtain:

$$\frac{\partial B}{\partial t} = \nabla\cdot\left[D_B\nabla B + \bar{v}W\left(B\frac{\partial v}{\partial B} + v\right)\nabla B + \bar{v}B\left(W\frac{\partial v}{\partial W} + v\right)\nabla W\right] - \lambda WB - \gamma_B\nabla^4 B$$

Note that inside the worm clusters, worm activity vanishes (v≈0) due to low oxygen levels, and outside the clusters, the density of worms vanishes (W≈0). Therefore, the bacterial velocity induced by worm activity creates a notable non-equilibrium flux only in the regions where the density of worms has a gradient.

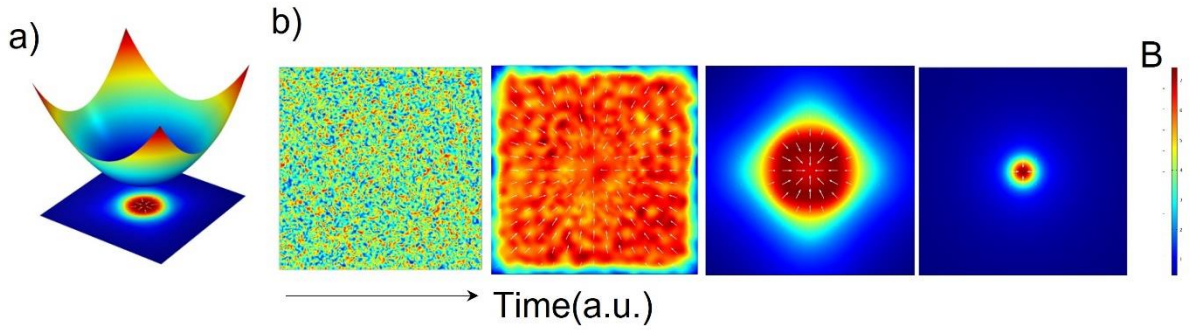

Supplementary Figure 3: Simulation results of aggregating passive particles under a spatial velocity profile. (a) A Gaussian-shaped spatial velocity profile (vertical axis) drives radial order and aggregation (horizontal plane). (b) Snapshots of aggregating passive particles. Arrows indicate the direction of the flux of the particles under the spatial activity gradient.

Furthermore, the activity of the worm inside and outside of the worm clusters can also be neglected as it does not create any significant flux due to the velocity of the bacteria becoming zero. Based on experimental observations and simulation results, for the simplicity of the model, we use the non-equilibrium flux term proportional to the gradient of the worm and the density of bacteria. Additionally, we assume that the diffusion of bacteria is constant. Therefore, we can finally write down this flux as follows

$$\overrightarrow{J_{neq}} = \zeta B \nabla W$$

where ζ is the term that determines the magnitude of the non-equilibrium flux of bacteria on the gradient of worm density. Finally, we can write down the time evolution equation of the bacteria density field as ;

$$\frac{\partial B}{\partial t} = \nabla \cdot [D_B \nabla B + \zeta B \nabla W] - \lambda W B - \gamma_B \nabla^4 B$$

III. Linear Stability Analysis

In the equilibrium state, worm and bacteria density is uniform over space and their time derivatives are also zero. Then we add a small perturbation to each of these fields.

$$W = W_{eq} + \delta W$$

$$B = B_{eq} + \delta B$$

With perturbed densities, we can write down the equation as follows with higher-order terms

$$\frac{\partial \delta W}{\partial t} = \nabla \cdot \left[D_{eff} \nabla \delta W + \beta \mathrm{W_{eq}} \nabla \delta B \right] - \gamma_W \nabla^4 \delta W$$

$$\frac{\partial \delta B}{\partial t} = \nabla \cdot \left[D_B \nabla \delta B + \zeta B_{eq} \nabla \delta W \right] - \lambda W_{eq} \delta B - \lambda B_{eq} \delta W - \gamma_B \nabla^4 \delta B$$

where effective diffusion and worm drift flux on bacteria density gradient is evaluated at their equilibrium

$$D_{eff} = \frac{v(W_{eq}, B_{eq})^2}{2\tau} + \frac{v(W_{eq}, B_{eq})}{\tau} \frac{\partial v(W_{eq}, B_{eq})}{\partial W}$$

$$\beta = \frac{v(W_{eq}, B_{eq})}{\tau} \frac{\partial v(W_{eq}, B_{eq})}{\partial B}$$

Now assume that perturbations of bacteria and worm density have the following single Fourier modes.

$$\delta W = \rho_W(t) e^{ikx}$$

$$\delta B = \rho_B(t) e^{ikx}$$

We can express the time evolution of the time-dependent part of the worm and bacteria density perturbations as a dynamical matrix form.

$$\frac{\partial}{\partial t} \begin{bmatrix} \rho_W \\ \rho_B \end{bmatrix} = \begin{bmatrix} -k^2 D_{eff} - k^4 \gamma_W & -k^2 \beta W_{eq} \\ -\lambda B_{eq} - k^2 \zeta B_{eq} & -\lambda W_{eq} - k^2 D_B - k^4 \gamma_B \end{bmatrix} \begin{bmatrix} \rho_W \\ \rho_B \end{bmatrix}$$

This dynamical equation can be simplified to a common form of;

$$\frac{\partial}{\partial t}\begin{bmatrix}\rho_W\\ \rho_B\end{bmatrix} = \begin{bmatrix}D_{WW} & D_{BW}\\ D_{WB} & D_{BB}\end{bmatrix}\begin{bmatrix}\rho_W\\ \rho_B\end{bmatrix}$$

where each term D_{WW}, D_{BW}, D_{WB}, D_{BB} represents the effect of worm to itself, bacteria to worm, worm to bacteria, and bacteria to itself respectively. Eigenvalues (σ) of the dynamical matrix reveal the characteristics of the system.

IV.Single Mode Approximation

The following section is particularly inspired by the analysis used to understand active and passive particle interactions performed by You.et.al. If we assume that our system is 1-D and apply periodic boundary conditions with the length of the domain being L, then the densities of the worm and bacteria fields can be decomposed into their Fourier components

$$\phi_W(x,t) = \sum_j \widehat{\phi_W^j}(t)\, e^{iq_j x}$$

$$\phi_B(x,t) = \sum_j \widehat{\phi_B^j}(t)\, e^{iq_j x}$$

$$q_j = \frac{2\pi}{L} j$$

in Fourier domain

$$\frac{\partial \phi_W}{\partial t} = \frac{\partial}{\partial x}\left[D_{eff}\frac{\partial}{\partial x}\phi_W + \beta\phi_W\frac{\partial}{\partial x}\phi_B\right] - \gamma_W\frac{\partial^4}{\partial x^4}\phi_W$$

$$\frac{\partial \phi_B}{\partial t} = \frac{\partial}{\partial x}\left[D_B\frac{\partial}{\partial x}\phi_B + \zeta\phi_B\frac{\partial}{\partial x}\phi_W\right] - \lambda\phi_W\phi_B - \gamma_B\frac{\partial^4}{\partial x^4}\phi_B$$

The important terms of these equations are

$$D_W = \frac{v^2}{2\tau}$$

$$\chi = \frac{v}{\tau}\frac{\partial v}{\partial W}$$

$$\beta = \frac{v}{\tau}\frac{\partial v}{\partial B}$$

Then we express the time evolution of the 1-D worm and bacterial density ϕ_W and ϕ_B as :

$$\frac{\partial \phi_W}{\partial t} = D_W \frac{\partial^2}{\partial x^2}\phi_W + \chi\left(\frac{\partial}{\partial x}\phi_W\right)^2 + \chi\phi_W \frac{\partial^2}{\partial x^2}\phi_W + \beta\phi_W \frac{\partial^2}{\partial x^2}\phi_B + \beta\left(\frac{\partial}{\partial x}\phi_W\right)\left(\frac{\partial}{\partial x}\phi_B\right) - \gamma_W \frac{\partial^4}{\partial x^4}\phi_W$$

$$\frac{\partial \phi_B}{\partial t} = D_B \frac{\partial^2}{\partial x^2}\phi_B + \zeta\left(\frac{\partial}{\partial x}\phi_B\right)\left(\frac{\partial}{\partial x}\phi_W\right) + \zeta\phi_B\left(\frac{\partial^2}{\partial x^2}\phi_W\right) - \lambda\phi_W\phi_B - \gamma_B \frac{\partial^4}{\partial x^4}\phi_B$$

Now, we can express these equations in the Fourier domain. While the linear terms can be dealt with directly and without complexity, the other terms demand the use of convolution. Initially, we provide a comprehensive expression for the convolution terms. However, with the application of the single-mode approximation, these terms will eventually be simplified. Our exploration commences with a detailed examination of the time evolution of each term in the worm density equation.

$$D_W \frac{\partial^2}{\partial x^2}\phi_W = D_W \sum_j -q_j^2 \widehat{\phi_W^j}\, e^{iq_j x}$$

$$\chi\left(\frac{\partial}{\partial x}\phi_W\right)^2 = \chi \sum_j \sum_{j_1} -q_{j_1} q_{j-j_1} \widehat{\phi_W^{j_1}}\, \widehat{\phi_W^{j-j_1}}\, e^{iq_j x}$$

$$\chi\phi_W\left(\frac{\partial^2}{\partial x^2}\phi_W\right) = \chi \sum_j \sum_{j_1} -q_{j_1}^2 \widehat{\phi_W^{j_1}}\, \widehat{\phi_W^{j-j_1}} e^{iq_j x}$$

$$\beta\phi_W\left(\frac{\partial^2}{\partial x^2}\phi_B\right) = \beta \sum_j \sum_{j_1} -q_{j_1}^2 \widehat{\phi_B^{j_1}}\, \widehat{\phi_W^{j-j_1}} e^{iq_j x}$$

$$\beta\left(\frac{\partial}{\partial x}\phi_W\right)\left(\frac{\partial}{\partial x}\phi_B\right) = \beta \sum_j \sum_{j_1} -q_{j_1} q_{j-j_1} \widehat{\phi_B^{j_1}}\, \widehat{\phi_W^{j-j_1}} e^{iq_j x}$$

$$\gamma_W \frac{\partial^4}{\partial x^4}\phi_W = \gamma_W \sum_j q_j^4 \widehat{\phi_W^j}\, e^{iq_j x}$$

If we bring those terms together we will have a very long-expression which gives us the time evolution of each Fourier series coefficient of the worm density.

$$\frac{\partial}{\partial t}\widehat{\phi_W^J} = -q_j^2 D_W \widehat{\phi_W^J} - \chi \sum_{j_1} q_{j_1} q_{j-j_1} \widehat{\phi_W^{j_1}} \widehat{\phi_W^{J-j_1}} - \chi \sum_{j_1} q_{j_1}^2 \widehat{\phi_W^{j_1}} \widehat{\phi_W^{J-j_1}} - \beta \sum_{j_1} q_{j_1}^2 \widehat{\phi_B^{j_1}} \widehat{\phi_W^{J-j_1}}$$

$$- \beta \sum_{j_1} q_{j_1} q_{j-j_1} \widehat{\phi_B^{j_1}} \widehat{\phi_W^{J-j_1}} - \gamma_W q_j^4 \widehat{\phi_W^J}$$

Now we repeat the similar process for the time evolution of the bacterial density

$$D_B \frac{\partial^2}{\partial x^2}\phi_B = D_B \sum_j -q_j^2 \widehat{\phi_B^J}\, e^{iq_j x}$$

$$\zeta \left(\frac{\partial}{\partial x}\phi_B\right)\left(\frac{\partial}{\partial x}\phi_W\right) = \zeta \sum_j \sum_{j_1} -q_{j_1} q_{j-j_1} \widehat{\phi_B^{j_1}} \widehat{\phi_W^{J-j_1}}\, e^{iq_j x}$$

$$\zeta \phi_B \left(\frac{\partial^2}{\partial x^2}\phi_W\right) = \zeta \sum_j \sum_{j_1} -q_{j_1}^2 \widehat{\phi_W^{j_1}}\, \widehat{\phi_B^{J-j_1}} e^{iq_j x}$$

$$\lambda \phi_W \phi_B = \lambda \sum_j \sum_{j_1} \widehat{\phi_W^{j_1}} \widehat{\phi_B^{J-j_1}} e^{iq_j x}$$

$$\gamma_B \frac{\partial^4}{\partial x^4}\phi_B = \sum_j q_j^4 \widehat{\phi_B^J} e^{iq_j x}$$

Arranging these terms together we find the time evolution of each of the Fourier coefficients of bacteria density

$$\frac{\partial}{\partial t}\widehat{\phi_B^J} = -q_j^2 D_B \widehat{\phi_B^J} - \zeta \sum_{j_1} q_{j_1} q_{j-j_1} \widehat{\phi_B^{j_1}} \widehat{\phi_W^{J-j_1}} - \zeta \sum_{j_1} q_{j_1}^2 \widehat{\phi_W^{j_1}} \widehat{\phi_B^{J-j_1}} - \lambda \sum_{j_1} \widehat{\phi_W^{j_1}} \widehat{\phi_B^{J-j_1}} - q_j^4 \gamma_B \widehat{\phi_B^J}$$

These equations include each coefficient of the Fourier series and include only periodic boundary condition assumptions. As a next step, we assume that domain length is $L = 2\pi$ for simplicity and make a single mode approximation which is $j = 0$ and $j = 1$ with all other modes equal to zero.

$$\widehat{\phi_W^J} = \widehat{\phi_B^J} = 0$$

In the following, we analyze the case of $j = 0$. The components of the Fourier coefficients become

$$\widehat{\phi_W^0} = \int_{<L>} \phi_W dx = \phi_W^0$$

$$\widehat{\phi_B^0} = \int_{<L>} \phi_B dx = \phi_B^0$$

For conserved fields, these components are constants, where worm density ϕ_W is a conserved quantity, but ϕ_B is not in our case which changes over time due to bacterial consumption by the worms, but for simplicity, we treat them as constant. By using these assumptions we rewrite the time evolution of the first Fourier coefficients As

$$\frac{\partial}{\partial t}\widehat{\phi_W^1} = -(q_1^2 D_W + q_1^4 \gamma_W + q_1^2 \chi \phi_W^0)\widehat{\phi_W^1} - q_1^2 \beta \phi_W^0 \widehat{\phi_B^1}$$

$$\frac{\partial}{\partial t}\widehat{\phi_B^1} = -(q_1^2 D_B + q_1^4 \gamma_B + \lambda \phi_w^0)\widehat{\phi_B^1} - (q_1^2 \zeta + \lambda)\phi_B^0 \widehat{\phi_W^1}$$

Note that both coefficients are complex. i.e., $\widehat{\phi_W^1}, \widehat{\phi_B^1} \in \mathbb{C}$. Therefore, they can be represented as :

$$\widehat{\phi_W^1}(t) = \rho_W(t) e^{i\theta_W(t)}$$

$$\widehat{\phi_B^1}(t) = \rho_B(t) e^{i\theta_B(t)}$$

$$\theta(t) = \theta_W(t) - \theta_B(t)$$

where both amplitudes $\rho_W(t), \rho_B(t) \in \mathbb{R}$ and phases $\theta_W(t), \theta_B(t) \in \mathbb{R}$. Using these equations, we write the time evolution of the amplitudes and phases as

$$\frac{\partial}{\partial t}\widehat{\phi_W^1} = e^{i\theta_W(t)}\left[\frac{\partial}{\partial t}\rho_W(t) + i\rho_W(t)\frac{\partial}{\partial t}\theta_W(t)\right]$$

$$\frac{\partial}{\partial t}\widehat{\phi_B^1} = e^{i\theta_B(t)}\left[\frac{\partial}{\partial t}\rho_B(t) + i\rho_B(t)\frac{\partial}{\partial t}\theta_B(t)\right]$$

$$\frac{\partial}{\partial t}\widehat{\phi_W^1} = e^{i\theta_W(t)}\left[-(q_1^2 D_W + q_1^4 \gamma_W + q_1^2 \chi \phi_W^0)\rho_W(t) - q_1^2 \beta \phi_W^0 \rho_B(t) e^{i(\theta_B(t) - \theta_W(t))}\right]$$

$$\frac{\partial}{\partial t}\widehat{\phi_B^1} = e^{i\theta_B(t)}[-(q_1^2 D_B + q_1^4 \gamma_B + \lambda \phi_w^0)\rho_B(t) - (q_1^2 \zeta + \lambda)\phi_B^0 \rho_W(t) e^{i(\theta_W(t) - \theta_B(t))}]$$

Now if we compose these equations we can find the time evolution of the both amplitudes and the phase of each worm and bacteria field:

$$\frac{\partial}{\partial t}\rho_W(t) = -(q_1^2 D_W + q_1^4 \gamma_W + q_1^2 \chi \phi_W^0)\rho_W(t) - q_1^2 \beta \phi_W^0 \rho_B(t)\cos(\theta)$$

$$\frac{\partial}{\partial t}\rho_B(t) = -(q_1^2 D_B + q_1^4 \gamma_B + \lambda \phi_w^0)\rho_B(t) - (q_1^2 \zeta + \lambda)\phi_B^0 \rho_W(t)\cos(\theta)$$

$$\frac{\partial}{\partial t}\theta_W(t) = q_1^2 \beta \phi_W^0 \frac{\rho_B(t)}{\rho_W(t)}\sin(\theta)$$

$$\frac{\partial}{\partial t}\theta_B(t) = -(q_1^2 \zeta + \lambda)\phi_B^0 \frac{\rho_W(t)}{\rho_B(t)}\sin(\theta)$$

Combing the last two equations yields a system of three coupled partial differential equations, which give the dynamics of the amplitudes and phase differences of the worm and bacteria fields as:

$$\frac{\partial}{\partial t}\rho_W(t) = -(q_1^2 D_W + q_1^4 \gamma_W + q_1^2 \chi \phi_W^0)\rho_W(t) - q_1^2 \beta \phi_W^0 \rho_B(t)\cos(\theta)$$

$$\frac{\partial}{\partial t}\rho_B(t) = -(q_1^2 D_B + q_1^4 \gamma_B + \lambda \phi_w^0)\rho_B(t) - (q_1^2 \zeta + \lambda)\phi_B^0 \rho_W(t)\cos(\theta)$$

$$\frac{\partial}{\partial t}\theta(t) = \left[q_1^2 \beta \phi_W^0 \frac{\rho_B(t)}{\rho_W(t)} + (q_1^2 \zeta + \lambda)\phi_B^0 \frac{\rho_W(t)}{\rho_B(t)}\right]\sin(\theta)$$

$$\frac{\partial}{\partial t}\Phi(t) = \left[q_1^2 \beta \phi_W^0 \frac{\rho_B(t)}{\rho_W(t)} - (q_1^2 \zeta + \lambda)\phi_B^0 \frac{\rho_W(t)}{\rho_B(t)}\right]\sin(\theta)$$

We can use the formalism at Section 2, to make further simplification and convert these equations to the common form

$$\frac{\partial \rho_W}{\partial t} = D_{WW}\rho_W + D_{BW}\rho_B\cos(\theta)$$

$$\frac{\partial \rho_B}{\partial t} = D_{WB}\rho_W\cos(\theta) + D_{BB}\rho_B$$

$$\frac{\partial \theta}{\partial t} = -\left[D_{BW}\frac{\rho_B}{\rho_W} + D_{WB}\frac{\rho_W}{\rho_B}\right]\sin(\theta)$$

$$\frac{\partial \Phi}{\partial t} = -\left[D_{BW}\frac{\rho_B}{\rho_W} - D_{WB}\frac{\rho_W}{\rho_B}\right]\sin(\theta)$$

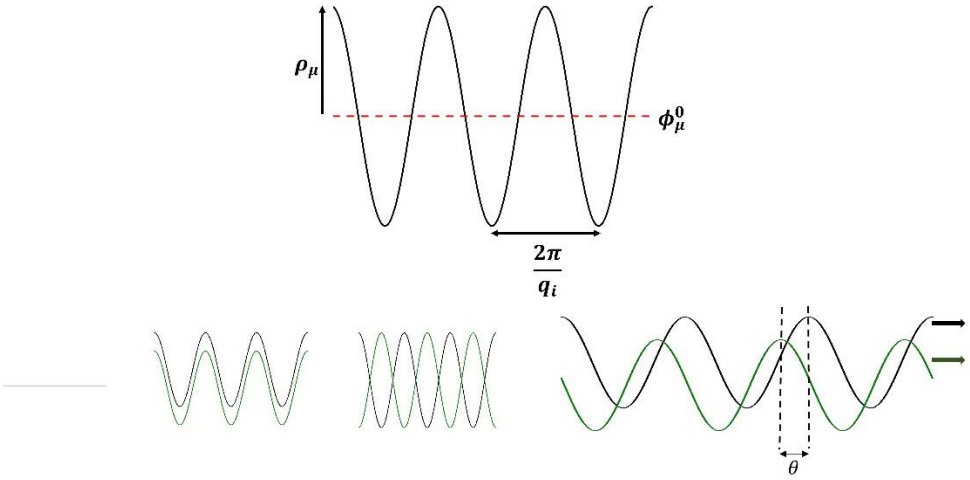

Supplementary Figure 4: **Schematic representation of single mode and the stability of the phase shift between interacting worm and bacterial fields. Stability of the phase shift drive uniform aligned antialigned and chiral phases.**

If we look at the stable solutions of this equation system. To have a constant phase difference ($\dot{\theta} = 0$) the first possibility is to satisfy $\sin(\theta) = 0$. There are two possible solutions, the first one is $\theta = 0$ and the second one is $\theta = \pi$ where they correspond to aligned (colocalized) and anti-aligned (delocalized) cases respectively (Supplementary Figure4). Note that when $\sin(\theta) = 0$, we also have that $\dot{\Phi} = 0$ which implies static patterns. Therefore, there are only two possible static cases, aligned and anti-aligned. Let's look at the solution for aligned case $\theta = 0$ and let the static solutions of the worm and bacteria field be ρ_W^s and ρ_B^s respectively, which is obtained as:

$$\frac{\rho_W^s}{\rho_B^s} = -\frac{D_{BW}}{D_{WW}}$$

$$\frac{\rho_W^s}{\rho_B^s} = -\frac{D_{BB}}{D_{WB}}$$

Note that ρ_W^s and ρ_B^s are amplitudes of the oscillations, therefore it is required that both of them should be positive. Therefore, for aligned stable solutions, the following equations should be satisfied:

718 $$D_{WW}D_{BB} - D_{BW}D_{WB} = 0$$

719 $$\frac{D_{BW}}{D_{WW}}, \frac{D_{BB}}{D_{WB}} < 0$$

720 If we look at the case $\theta = \pi$, which is the anti-aligned case, we will have similar conditions. It is

721 possible to generalize the stable static solution condition as below. If the condition,

722 $$D_{WW}D_{BB} - D_{BW}D_{WB} = 0$$

723 is satisfied, then there is a stable solution with the following rate of amplitudes.

724 $$\frac{\rho_W^s}{\rho_B^s} = \left|\frac{D_{BW}}{D_{WW}}\right|$$

725 The stable phase difference is also given below.

726 $$\frac{D_{BB}}{D_{WB}} < 0\,, \qquad \theta^s = 0$$

727 $$\frac{D_{BB}}{D_{WB}} > 0, \;\; \theta^s = \pi$$

728 As a next step, we look for another family of solutions with constant phase amplitudes and constant

729 phase difference and $\sin(\theta) \neq 0$. The condition to have a constant phase difference is

730 $$D_{BW}\frac{\rho_B^T}{\rho_W^T} + D_{WB}\frac{\rho_W^T}{\rho_B^T} = 0$$

731 where ρ_W^T and ρ_B^T are constant amplitudes of traveling worm and bacteria density respectively.

732 Satisfying this condition implies that there is a non-zero angular velocity of phases $\omega = \frac{\dot{\Phi}}{2}$. Note

733 that the amplitudes are also constant, thus we will have the following equations.

734 $$\frac{\rho_W^T}{\rho_B^T} = -\frac{D_{BW}}{D_{WW}}\cos(\theta^T)$$

735 $$\frac{\rho_W^T}{\rho_B^T} = -\frac{D_{BB}}{D_{WB}}\frac{1}{\cos(\theta^T)}$$

736 Finally, we have an expression for the phase difference between worm and bacteria fields for the

737 traveling (chiral) state which indicates the PT symmetry breaking.

$$\cos(\theta^T) = \pm\sqrt{\frac{D_{WW}D_{BB}}{D_{BW}D_{WB}}}$$

If we insert constant amplitude conditions into constant phase difference conditions, we can have the following equality with the condition $D_{BW}, D_{WB} \neq 0$. In addition, we need to satisfy that $0 \leq \cos(\theta^T) \leq 1$, in order to have a physical solution. Therefore, our final conditions to observe traveling wave solution with constant amplitude and the phase difference is

$$D_{WW} + D_{BB} = 0$$

$$0 < \frac{D_{WW}D_{BB}}{D_{BW}D_{WB}} \leq 1$$

Note that these conditions can only be satisfied with self-aggregating anmimals (negative effective diffusion of the worms) together with the nonreciprocity term (sufficient λ) and the angular velocity of phases.

$$\omega = \frac{1}{2}(D_{WW} - D_{BB})\tan(\theta^T)$$

V.Travelling Region as PT Symmetry Breaking

Linear stability analysis of the system reveals that there is a curve that separates PT-exact and PT-broken regions. Points of this curve are called exceptional points. In this section, we will investigate this PT-exact and PT-broken region with parity and time inversion of eigenvectors of dynamical matrix M. The following calculations were used to analyze the PT symmetry breaking process of Kelvin-Helmholtz instability by H.Qin et.al. [52] . We applied the similar procedure to find the common form of PT operator starting from the linearized dynamical matrix form,

$$\frac{\partial}{\partial t}\begin{bmatrix}\rho_W \\ \rho_B\end{bmatrix} = M\begin{bmatrix}\rho_W \\ \rho_B\end{bmatrix}$$

$$M = \begin{bmatrix}D_{WW} & D_{BW} \\ D_{WB} & D_{BB}\end{bmatrix}$$

This dynamical matrix is written for the basis given below.

$$v_1 = \begin{bmatrix} e^{ikx} \\ 0 \end{bmatrix}, v_2 = \begin{bmatrix} 0 \\ e^{ikx} \end{bmatrix}$$

An important point is that these basis vectors are invariant under PT transformation. Where $x \to -x$ and $i \to -i$, then $v_1 \to v_1$ and $v_2 \to v_2$. Therefore, general PT transformation is multiplying the vector or matrix from left by P (parity matrix) and complex conjugation (time reversal). For this basis, P is the identity matrix.

$$P = \begin{bmatrix} 1 & 0 \\ 0 & 1 \end{bmatrix}$$

Now let's look at the eigenvalues and eigenvectors of M, which are $\lambda_{+,-}$ and $v_{+,-}$.

$$\lambda_{\pm} = \frac{1}{2}(D_{WW} + D_{BB}) \pm \frac{1}{2}\sqrt{(D_{WW} - D_{BB})^2 + 4D_{WB}D_{BW}}$$

The region with $(D_{WW} - D_{BB})^2 + 4D_{WB}D_{BW} > 0$ is characterized by two distinct real eigenvalues where $\lambda_{\pm} \in \mathbb{R}$, and is called the PT-exact regime. In this case $M \in \mathbb{R}^{2x2}$ implies that $v_{\pm} \in \mathbb{R}^2$. First note that M is a real matrix, therefore it is PT symmetric.

$$M \overset{PT}{\to} M$$

Having real eigenvectors, also implies that they are PT symmetric in this basis.

$$v_{\pm} \overset{PT}{\to} v_{\pm}$$

The region $(D_{WW} - D_{BB})^2 + 4D_{WB}D_{BW} < 0$ is the broken-PT phase characterized by two complex conjugate eigenvalues where $\lambda_{\pm} \in \mathbb{C}$ and $\overline{\lambda_+} = \lambda_-$. Noting that $M \in \mathbb{R}^{2x2}$, we find $\overline{v_+} = v_-$ which implies that in the PT-broken phase eigenvectors are mapped to each other under PT transformation which shows the spontaneous breaking of PT symmetry.

$$v_{\pm} \overset{PT}{\to} v_{\mp}$$

If we change the basis, we can obtain a different parity transformation matrix P. Let's use the following basis.

$$v_1 = \begin{bmatrix} ie^{ikx} \\ 0 \end{bmatrix}, v_2 = \begin{bmatrix} 0 \\ e^{ikx} \end{bmatrix}$$

This basis convention is equivalent to the following perturbation to uniform equilibrium worm and bacteria densities.

$$\delta W = \rho_W(t) ie^{ikx}$$

$$\delta B = \rho_B(t) e^{ikx}$$

If we use these perturbations in our main equations and use D_{WW}, D_{BW}, D_{WB}, D_{BB} as before we will have the dynamical matrix M' in a new basis as given below.

$$M' = \begin{bmatrix} D_{WW} & -iD_{BW} \\ iD_{WB} & D_{BB} \end{bmatrix}$$

We can see that eigenvalues are the same as the previous basis which are given below.

$$\lambda_{\pm}{}' = \frac{1}{2}(D_{WW} + D_{BB}) \pm \frac{1}{2}\sqrt{(D_{WW} - D_{BB})^2 + 4D_{WB}D_{BW}}$$

This is an expected result because the change of basis doesn't change eigenvalues but it changes the eigenvectors and importantly it changes parity transformation P in our case. Note that because eigenvalues didn't change, PT-exact and PT-broken regions are also the same. Let's first look at the eigenvectors of the M'.

$$v_{\pm}{}' = \begin{bmatrix} iD_{BB} - i\lambda_{\pm} \\ D_{WB} \end{bmatrix}$$

Now let's look at our basis vectors and find the corresponding parity transformation matrix P.

$$v_1 = \begin{bmatrix} ie^{ikx} \\ 0 \end{bmatrix}$$

$$v_2 = \begin{bmatrix} 0 \\ e^{ikx} \end{bmatrix}$$

If we apply the PT transformation, we have the following transformation of basis vectors.

$$v_1 \overset{PT}{\rightarrow} -v_1$$

$$v_2 \overset{PT}{\rightarrow} v_2$$

Then we finally have found the new parity transformation in this basis let it be P'.

$$P' = \begin{bmatrix} -1 & 0 \\ 0 & 1 \end{bmatrix}$$

In PT-exact region, $\lambda_\pm \in \mathbb{R}$, which implies the following PT transformation.

$${v_\pm}' \overset{PT}{\rightarrow} {v_\pm}'$$

This shows us that in the PT-exact region, PT transformation eigenvectors to itself. Now investigate the PT-broken region where $\lambda_\pm \in \mathbb{C}$ where $\overline{\lambda_\pm} = \lambda_\mp$. Now if we look at the transformation

$$P'\overline{v'_\pm} = \begin{bmatrix} iD_{BB} - i\lambda_\mp \\ D_{WB} \end{bmatrix}$$

Finally, we showed that in the PT-broken region with a given basis, PT transformation maps eigenvectors to each other.

$$v'_\pm \overset{PT}{\rightarrow} v'_\mp$$

These parity transformation matrices are still not the same as the usual transformation P we are used to from quantum mechanics. In order to obtain the same parity transformation matrix, apply the following transformation Q to the altered dynamical matrix M'.

$$Q = \frac{1}{\sqrt{2}}\begin{bmatrix} -1 & 1 \\ 1 & 1 \end{bmatrix}$$

Again, changing the basis with transformation matrix Q doesn't change the eigenvalues. But new eigenvectors are $v_\pm = Qv'_\pm$. The new dynamical matrix becomes $QM'Q^{-1}$ and new parity operator P is $QP'Q^{-1}$.

$$P = \begin{bmatrix} 0 & 1 \\ 1 & 0 \end{bmatrix}$$

$$v_\pm = \frac{1}{\sqrt{2}}\begin{bmatrix} D_{WB} - i(D_{BB} - \lambda_\pm) \\ D_{WB} + i(D_{BB} - \lambda_\pm) \end{bmatrix}$$

Now in the PT-exact region, we have that $\lambda_{\pm} \in \mathbb{R}$, which implies that with given P and complex conjugation together each eigenvector is mapped to itself.

$$P\overline{v_{\pm}} = \frac{1}{\sqrt{2}}\begin{bmatrix}0 & 1\\ 1 & 0\end{bmatrix}\begin{bmatrix}D_{WB} + i(D_{BB} - \lambda_{\pm})\\ D_{WB} - i(D_{BB} - \lambda_{\pm})\end{bmatrix} = \frac{1}{\sqrt{2}}\begin{bmatrix}D_{WB} - i(D_{BB} - \lambda_{\pm})\\ D_{WB} + i(D_{BB} - \lambda_{\pm})\end{bmatrix}$$

$$v_{\pm} \overset{PT}{\rightarrow} v_{\pm}$$

If we look at the PT-broken region where $\lambda_{\pm} \in \mathbb{C}$ and $\overline{\lambda_{\pm}} = \lambda_{\mp}$.

$$P\overline{v_{\pm}} = \frac{1}{\sqrt{2}}\begin{bmatrix}0 & 1\\ 1 & 0\end{bmatrix}\begin{bmatrix}D_{WB} + i(D_{BB} - \lambda_{\mp})\\ D_{WB} - i(D_{BB} - \lambda_{\mp})\end{bmatrix} = \frac{1}{\sqrt{2}}\begin{bmatrix}D_{WB} - i(D_{BB} - \lambda_{\mp})\\ D_{WB} + i(D_{BB} - \lambda_{\mp})\end{bmatrix}$$

$$v_{\pm} \overset{PT}{\rightarrow} v_{\mp}$$

In this regime, PT transformation maps eigenvectors to each other which explicitly shows the PT breaking in the traveling regime.

References

Uncategorized References

1 Bowick, M. J., Fakhri, N., Marchetti, M. C. & Ramaswamy, S. Symmetry, Thermodynamics, and Topology in Active Matter. *Phys Rev X* **12**, doi:ARTN 010501

10.1103/PhysRevX.12.010501 (2022).

2 Marchetti, M. C. *et al.* Hydrodynamics of soft active matter. *Rev Mod Phys* **85**, doi:ARTN 1143

10.1103/RevModPhys.85.1143 (2013).

3 Fruchart, M., Hanai, R., Littlewood, P. B. & Vitelli, V. Non-reciprocal phase transitions. *Nature* **592**, doi:10.1038/s41586-021-03375-9 (2021).

4 You, Z. H., Baskaran, A. & Marchetti, M. C. Nonreciprocity as a generic route to traveling states. *P Natl Acad Sci USA* **117**, 19767-19772, doi:10.1073/pnas.2010318117 (2020).

5 Saha, S., Agudo-Canalejo, J. & Golestanian, R. Scalar Active Mixtures: The Nonreciprocal Cahn-Hilliard Model. *Phys Rev X* **10**, doi:ARTN 041009

10.1103/PhysRevX.10.041009 (2020).

6 Gupta, R. K., Kant, R., Soni, H., Sood, A. K. & Ramaswamy, S. Active nonreciprocal attraction between motile particles in an elastic medium. *Phys Rev E* **105**, doi:ARTN 064602

10.1103/PhysRevE.105.064602 (2022).

7 Chen, Y. Y., Li, X. P., Scheibner, C., Vitelli, V. & Huang, G. L. Realization of active metamaterials with odd micropolar elasticity. *Nature Communications* **12**, doi:ARTN 5935

10.1038/s41467-021-26034-z (2021).

8 Biktashev, V. N. & Tsyganov, M. A. Spontaneous traveling waves in oscillatory systems with cross diffusion. *Phys Rev E* **80**, doi:ARTN 056111

10.1103/PhysRevE.80.056111 (2009).
9 Tan, T. H. *et al.* Odd dynamics of living chiral crystals. *Nature* **607**, 287-+, doi:10.1038/s41586-022-04889-6 (2022).
10 Dinelli, A. *et al.* Non-reciprocity across scales in active mixtures. *Nat Commun* **14**, 7035, doi:10.1038/s41467-023-42713-5 (2023).
11 Ivlev, A. V. *et al.* Statistical Mechanics where Newton's Third Law is Broken. *Phys Rev X* **5**, doi:ARTN 011035

10.1103/PhysRevX.5.011035 (2015).
12 Soleymani, S. *et al.* Chiral and degenerate perfect absorption on exceptional surfaces. *Nature Communications* **13**, doi:ARTN 599

10.1038/s41467-022-27990-w (2022).
13 Zhong, Q. *et al.* Sensing with Exceptional Surfaces in Order to Combine Sensitivity with Robustness. *Physical Review Letters* **122**, doi:ARTN 153902

10.1103/PhysRevLett.122.153902 (2019).
14 Lau, H. K. & Clerk, A. A. Fundamental limits and non-reciprocal approaches in non-Hermitian quantum sensing. *Nature Communications* **9**, doi:ARTN 4320

10.1038/s41467-018-06477-7 (2018).
15 Bender, C. M. & Boettcher, S. Real spectra in non-Hermitian Hamiltonians having PT symmetry. *Physical Review Letters* **80**, 5243-5246, doi:DOI 10.1103/PhysRevLett.80.5243 (1998).
16 Hatano, N. & Nelson, D. R. Localization transitions in non-Hermitian quantum mechanics. *Physical Review Letters* **77**, 570-573, doi:DOI 10.1103/PhysRevLett.77.570 (1996).
17 Ozdemir, S. K., Rotter, S., Nori, F. & Yang, L. Parity-time symmetry and exceptional points in photonics. *Nat Mater* **18**, 783-798, doi:10.1038/s41563-019-0304-9 (2019).
18 El-Ganainy, R. *et al.* Non-Hermitian physics and PT symmetry. *Nat Phys* **14**, 11-19, doi:10.1038/Nphys4323 (2018).
19 Miri, M. A. & Alù, A. Exceptional points in optics and photonics. *Science* **363**, 42-+, doi:ARTN eaar7709

10.1126/science.aar7709 (2019).
20 Naghiloo, M., Abbasi, M., Joglekar, Y. N. & Murch, K. W. Quantum state tomography across the exceptional point in a single dissipative qubit. *Nat Phys* **15**, 1232-+, doi:10.1038/s41567-019-0652-z (2019).
21 Zhang, J. W. *et al.* Dynamical control of quantum heat engines using exceptional points. *Nature Communications* **13**, doi:ARTN 6225

10.1038/s41467-022-33667-1 (2022).
22 Ding, L. Y. *et al.* Experimental Determination of

-Symmetric Exceptional Points in a Single Trapped Ion. *Physical Review Letters* **126**, doi:ARTN 083604

10.1103/PhysRevLett.126.083604 (2021).
23 Wu, Y. *et al.* Observation of parity-time symmetry breaking in a single-spin system. *Science* **364**, 878-+, doi:10.1126/science.aaw8205 (2019).
24 Ergoktas, M. S. *et al.* Topological engineering of terahertz light using electrically tunable exceptional point singularities. *Science* **376**, 184-+, doi:10.1126/science.abn6528 (2022).
25 Zhou, Z. C. *et al.* Prospects and applications of on-chip lasers. *Elight* **3**, doi:ARTN 1

10.1186/s43593-022-00027-x (2023).
26 Huang, R. *et al.* Exceptional Photon Blockade: Engineering Photon Blockade with Chiral Exceptional Points. *Laser Photonics Rev* **16**, doi:ARTN 2100430

10.1002/lpor.202100430 (2022).
27 Rogers, C., Persson, A., Cheung, B. & de Bono, M. Behavioral motifs and neural pathways coordinating O2 responses and aggregation in C. elegans. *Curr Biol* **16**, 649-659, doi:10.1016/j.cub.2006.03.023 (2006).
28 Gray, J. M. *et al.* Oxygen sensation and social feeding mediated by a C-elegans guanylate cyclase homologue. *Nature* **430**, 317-322, doi:10.1038/nature02714 (2004).
29 de Bono, M. & Bargmann, C. I. Natural variation in a neuropeptide Y receptor homolog modifies social behavior and food response in C-elegans. *Cell* **94**, 679-689, doi:Doi 10.1016/S0092-8674(00)81609-8 (1998).
30 Zimmer, M. *et al.* Neurons Detect Increases and Decreases in Oxygen Levels Using Distinct Guanylate Cyclases. *Neuron* **61**, 865-879, doi:10.1016/j.neuron.2009.02.013 (2009).
31 Zhao, Y. *et al.* Changes to social feeding behaviors are not sufficient for fitness gains of the Caenorhabditis elegans N2 reference strain. *Elife* **7**, doi:10.7554/eLife.38675 (2018).
32 Demir, E., Yaman, Y. I., Basaran, M. & Kocabas, A. Dynamics of pattern formation and emergence of swarming in Caenorhabditis elegans. *Elife* **9**, doi:ARTN e52781

10.7554/eLife.52781 (2020).
33 Tiribocchi, A., Wittkowski, R., Marenduzzo, D. & Cates, M. E. Active Model H: Scalar Active Matter in a Momentum-Conserving Fluid. *Physical Review Letters* **115**, doi:ARTN 188302

10.1103/PhysRevLett.115.188302 (2015).
34 Tjhung, E., Nardini, C. & Cates, M. E. Cluster Phases and Bubbly Phase Separation in Active Fluids: Reversal of the Ostwald Process. *Phys Rev X* **8**, doi:ARTN 031080

10.1103/PhysRevX.8.031080 (2018).
35 Stenhammar, J., Wittkowski, R., Marenduzzo, D. & Cates, M. E. Light-induced self-assembly of active rectification devices. *Sci Adv* **2**, doi:ARTN e1501850

10.1126/sciadv.1501850 (2016).
36 Guzmán-Lastra, F., Löwen, H. & Mathijssen, A. J. T. M. Active carpets drive non-equilibrium diffusion and enhanced molecular fluxes. *Nature Communications* **12**, 1906, doi:10.1038/s41467-021-22029-y (2021).
37 Schnitzer, M. J. Theory of Continuum Random-Walks and Application to Chemotaxis. *Phys Rev E* **48**, 2553-2568, doi:DOI 10.1103/PhysRevE.48.2553 (1993).
38 Almonacid, M. *et al.* Active diffusion positions the nucleus in mouse oocytes. *Nat Cell Biol* **17**, 470-+, doi:10.1038/ncb3131 (2015).
39 Colin, A. *et al.* Active diffusion in oocytes nonspecifically centers large objects during prophase I and meiosis I. *J Cell Biol* **219**, doi:ARTN e201908195

10.1083/jcb.201908195 (2020).
40 Ramm, B. *et al.* A diffusiophoretic mechanism for ATP-driven transport without motor proteins. *Nat Phys*, doi:10.1038/s41567-021-01213-3 (2021).
41 Stenhammar, J., Wittkowski, R., Marenduzzo, D. & Cates, M. E. Activity-Induced Phase Separation and Self-Assembly in Mixtures of Active and Passive Particles. *Physical Review Letters* **114**, doi:ARTN 018301

10.1103/PhysRevLett.114.018301 (2015).

42 Cates, M. E., Marenduzzo, D., Pagonabarraga, I. & Tailleur, J. Arrested phase separation in reproducing bacteria creates a generic route to pattern formation. *P Natl Acad Sci USA* **107**, 11715-11720, doi:10.1073/pnas.1001994107 (2010).
43 Cates, M. E. & Tailleur, J. Motility-Induced Phase Separation. *Annu Rev Conden Ma P* **6**, 219-244, doi:10.1146/annurev-conmatphys-031214-014710 (2015).
44 Mostafazadeh, A. Pseudo-Hermiticity versus symmetry:: The necessary condition for the reality of the spectrum of a non-Hermitian Hamiltonian. *J Math Phys* **43**, 205-214, doi:Doi 10.1063/1.1418246 (2002).
45 Nelson, D. R. & Shnerb, N. M. Non-Hermitian localization and population biology. *Phys Rev E* **58**, 1383-1403, doi:DOI 10.1103/PhysRevE.58.1383 (1998).
46 Shen, H. T., Zhen, B. & Fu, L. Topological Band Theory for Non-Hermitian Hamiltonians. *Physical Review Letters* **120**, doi:ARTN 146402 10.1103/PhysRevLett.120.146402 (2018).
47 Dasbiswas, K., Mandadapu, K. K. & Vaikuntanathan, S. Topological localization in out-of-equilibrium dissipative systems. *P Natl Acad Sci USA* **115**, E9031-E9040, doi:10.1073/pnas.1721096115 (2018).
48 Murugan, A. & Vaikuntanathan, S. Topologically protected modes in non-equilibrium stochastic systems. *Nature Communications* **8**, doi:ARTN 13881 10.1038/ncomms13881 (2017).
49 Tang, E., Agudo-Canalejo, J. & Golestanian, R. Topology Protects Chiral Edge Currents in Stochastic Systems. *Phys Rev X* **11**, doi:ARTN 031015 10.1103/PhysRevX.11.031015 (2021).
50 Brenner, M. P., Levitov, L. S. & Budrene, E. O. Physical mechanisms for chemotactic pattern formation by bacteria. *Biophysical Journal* **74**, 1677-1693, doi:Doi 10.1016/S0006-3495(98)77880-4 (1998).
51 Cummins, H. Z., Fourtune, L. & Rabaud, M. Successive Bifurcations in Directional Viscous Fingering. *Phys Rev E* **47**, 1727-1738, doi:DOI 10.1103/PhysRevE.47.1727 (1993).
52 Qin, H., Zhang, R. L., Glasser, A. S. & Xiao, J. Y. Kelvin-Helmholtz instability is the result of parity-time symmetry breaking. *Phys Plasmas* **26**, doi:Artn 032102 10.1063/1.5088498 (2019).

Supplementary Files

This is a list of supplementary files associated with this preprint. Click to download.

- Video1.avi
- Video2.mp4
- Video3.avi
- Video4.mp4
- Video5.avi
- Video6.avi
- Video7.avi
- Video8.avi
- Video9.avi
- Video10.avi
- Video11.avi
- Video12.avi